PHOTONICS Research

Laser-driven self-exfoliation of graphene oxide layers on a fiber facet for Q switching of an Er-doped fiber laser at the longest wavelength

Byungjoo Kim,[1] Seongjin Hong,[1] Jaedeok Park,[2] Yongsoo Lee,[1] Dong-il Yeom,[2] and Kyunghwan Oh[1,*]

[1]Photonic Device Physics Laboratory, Institute of Physics and Applied Physics, Yonsei University, Seoul 03722, South Korea
[2]Department of Physics and Energy Systems Research, Ajou University, Suwon 16499, South Korea
*Corresponding author: koh@yonsei.ac.kr

Received 1 May 2020; revised 11 June 2020; accepted 12 June 2020; posted 12 June 2020 (Doc. ID 396566); published 17 July 2020

A new method to make an all-fiber nonlinear optic device for laser pulse generation is developed by depositing multi-layer graphene oxide (GO) selectively onto the core of the cleaved fiber facet by combining the electrical arc discharge and the laser-driven self-exfoliation. Using the GO colloid droplet with sub-nanoliter volume, we obtained a GO bulk layer deposited on a fiber facet of the order of milliseconds by using an electric arc. The prepared fiber facet was then included in an Er-doped fiber laser (EDFL) cavity and we obtained a few layers of GO having nonlinear optic two-dimensional (2D) characteristics selectively on the fiber core by the laser-driven self-exfoliation. The 2D GO layers on the fiber core served as a stable and efficient saturable absorber enabling robust pulse train generation at $\lambda = 1600.5$ nm, the longest Q-switched laser wavelength in EDFLs. Pulse characteristics were analyzed as we varied the pump power at $\lambda = 980$ nm from 105.2 mW to 193.6 mW, to obtain the maximum repetition rate of 17.8 kHz and the maximum output power of 2.3 mW with the minimum pulse duration of 7.8 μs. The proposed method could be further applied to other novel inorganic 2D materials opening a window to explore their novel nonlinear optic laser applications.

https://doi.org/10.1364/PRJ.396566

1. INTRODUCTION

In recent decades, researchers have endeavored continuous efforts in developing ultrafast pulsed lasers utilizing novel light interactions with novel materials such as two-dimensional (2D) matters including transition metal dichalcogenides (TMDs), topological insulator, and black phosphorus [1–6]. Among these, a family of carbon-based materials including graphene and carbon nanotubes has been successfully applied to Q switching and mode-locking of lasers [7–11]. Graphene oxide (GO) has been recently adopted as a saturable absorber (SA) with high optical nonlinearity and a chemically stable 2D structure to generate short pulses in various laser cavities [12–25]. Compact and reliable integration of these novel materials into fiber-optic components has been a critical issue to make all-fiber pulsed lasers and several methods have been demonstrated to realize fiber-optic SAs. Depending on substrates where the materials were deposited, there have been attempts such as deposition on the cleaved fiber facet [2], the outer surface of a tapered fiber [3,4], and the surface of a side-polished fiber [1,5], to name a few. For these substrates, various deposition methods have been subsequently developed, including optical deposition [26], liquid precursor spraying [22], drop-casting [27], spin-coating [1,5], transfer of mechanically exfoliated materials [28], and polymer composite thin films [29,30]. However, these prior methods have required significant amounts of precursors, elaborated optimization procedures, and limited spatial selectivity in the film deposition, which has been a practical limit for fiber-optic device applications.

In this study, an innovative way of depositing multi-layer GO selectively on the core of the cleaved facet of a single-mode fiber (SMF) was proposed to make a compact all-fiber SA for Er-doped fiber laser (EDFL) Q switching. The notions of the novelty in the proposed method are as follows: (1) the volume of the liquid precursor used was less than 0.5 nL, the smallest volume ever reported in comparison with ∼2 μL or more in prior reports [4]; (2) simultaneous solvent evaporation and deposition of solid GO bulk layer were achieved in a few milliseconds using an electric arc, the shortest process time ever reported in comparison with ∼10 min or longer [27]; and (3) highly nonlinear multi-layer GO film SA was further achieved by self-starting Q-switched pulses selectively only at the fiber core with the diameter of ∼10 μm providing a high level of spatial directivity and resolution in the deposition process.

A schematic diagram of the proposed process is shown in Fig. 1. We constructed a ring laser cavity using an Er-doped

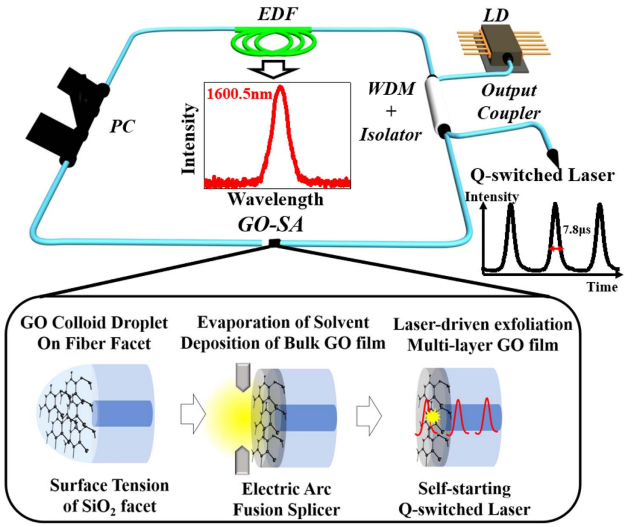

Fig. 1. Schematic diagram of the proposed deposition process and Q switching of an Er-doped fiber laser using a graphene oxide saturable absorber. The inset shows the three steps in the proposed GO deposition by using the electric arc and self-starting Q-switched laser pulses. (LD, pump laser diode at $\lambda = 980$ nm; PC, polarization controller; EDF, Er-doped fiber; WDM, 980 nm/1550 nm wavelength-division multiplexer; GO-SA, graphene oxide saturable absorber.)

fiber (EDF) as a gain medium pumped by a laser diode (LD) at $\lambda = 980$ nm. The laser output was obtained through one of the arms of a wavelength-division multiplexer (WDM). A fiber-optic GO-SA was formed on a cleaved facet of an SMF in the following three steps. (1) A drop of the aqueous colloid, where GO flakes were uniformly dispersed, was formed on the cleaved facet of an SMF by dipping its end to the colloid. See the left figure in the inset of Fig. 1. (2) The prepared SMF with a GO droplet was mounted on a commercial fusion splicer. Using an optimal condition, we simultaneously achieved evaporation of the solvent in the droplet and deposition of bulk GO film on the entire fiber facet by a single electric arc, as shown in the middle of the inset diagram. (3) The bulk GO film deposited fiber was inserted into the ring laser cavity. At an optimal gap between the GO deposited fiber and a pristine SMF, the self-starting Q-switched laser pulses exfoliated the GO flakes selectively only at the core to form a multi-layer GO film SA, which resulted in a stable pulse train generation. See the right figure in the inset.

In comparison to prior deposition processes [1,5,26–30], our new deposition technique can provide both a low insertion loss of 0.6 dB and a high modulation depth of ~3.7%. This unique combination provided a stable Q switching at the longest L-band wavelength. Furthermore, the process is optimized to the optical fiber facet substrates, which can readily provide all-fiber 2D material device platforms. Using this newly developed technique, we fabricated an all-fiber GO-SA and successfully achieved the Q switching of the EDFL in the L-band by using the proposed laser-driven self-exfoliation. In contrast to C-band EDFLs [2–6,9], studies on Q switching in the L-band have been very scarce, despite the inherently broadband operating range of novel 2D SA materials. Using our method, we succeeded in generating stable Q-switched pulse trains at $\lambda = 1600.5$ nm, the longest wavelength ever reported in the Q switching of EDFL using 2D material to our best knowledge. A detailed description of the proposed process and characterization of the laser follows in the next sections.

2. METHODS

A. Deposition of GO Bulk Film and Multi-Layer on the Fiber Facet

In prior reports for GO thin films, colloidal suspension precursors have been used for spin-coating [19] or drop-casting processes [18,24] with optimal GO nanoflake concentrations and solvent compositions. In our study, we purchased a commercially available aqueous colloidal solution where GO nanoflakes were dispersed (Graphene Square Inc.). The commercial product had a standard GO nanoflake concentration of ~0.1% (mass fraction), which was optimized for homogeneous dispersion of flakes in the colloidal suspension. However, the concentration was too low for the electric arc deposition process and we reduced the amount of the solvent by slowly heating the colloid to reach the optimal ~0.75% (mass fraction). The solution was then vigorously stirred to keep a uniform dispersion of GO flakes for the following processes. Single-mode fiber (Corning SMF-28) was cleaved at 90°, and its facet was dipped into the prepared solution and quickly drawn out. Due to the hydrophilic nature of the silica fiber facet, a droplet was formed on it with a maximum height of ~62.5 μm and a contact angle of ~26.8° [31]. See the "left" figure in the inset of the schematic diagram in Fig. 1. Note that the volume of the GO solution was less than 0.5 nL, which is the least liquid precursor consumption ever reported.

The SMF with GO solution droplet was mounted in a fusion splicer (Fitel S177a) along with another bare SMF cleaved at 90°. We optimized the arc power and the arc duration to achieve simultaneously evaporation of the solvent and deposition of bulk GO film, as shown in Fig. 2(a). We used the "Clean Arc Program" provided by the splicer and we found the arc power of 10 out of 128 with the arc duration of 10 ms was optimal for our purpose. The absolute arc power was not available since the splicer supplier, Fitel, did not provide the related information. The scanning electron microscope (SEM) image of the deposited GO bulk film is shown in Fig. 2(b). The optical microscopic image is also presented in the inset. In those images, we confirmed that the GO bulk film covered most of the fiber facet area with a diameter of 125 μm. The GO bulk film thickness was estimated to be ~2 μm similar to a prior report [32]. On the other SMF mounted in the fusion splicer, we did not observe any trace of GO flakes, and the deposition of GO bulk film was selectively achieved on the fiber facet where the precursor drop was placed.

The gap between the bulk GO deposited fiber facet and the pristine fiber facet, denoted as "d" in Fig. 2(a), was further optimized near ~8 μm to achieve two goals: (1) the laser-driven self-exfoliation process to result in a few layers of GO on the fiber core, and (2) Fabry–Perot filter for selecting the lasing wavelength in the L-band. By slowly increasing the pump laser power, we observed unstable Q switching and continuous wave (CW) sporadically. As we further increased the pump power,

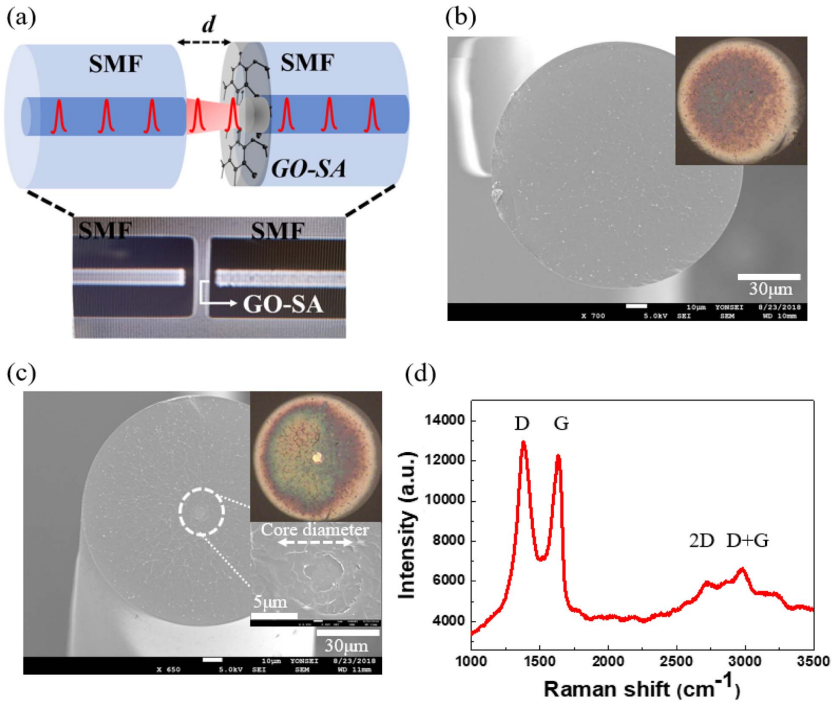

Fig. 2. (a) Configuration of the fabricated all-fiber GO-SA. The inset picture was taken from the fusion splicer. The gap between two fiber facets, *d*, was optimized to be ~8 μm. (b) Scanning electron microscope (SEM) image of the GO bulk film on the fiber facet deposited by the electric arc. Inset is its optical microscopic image. (c) SEM images of the GO multi-layer film on the fiber facet formed by laser-driven self-exfoliation. The blown SEM image clearly shows a layered structure on the fiber core. The inset is its optical microscopic image, where the light was guided through the core with a significantly thinner GO multi-layer film. (d) Micro Raman spectrum of the deposited GO film on the fiber core after the laser-driven self-exfoliation. (SMF, single mode fiber; GO-SA, graphene oxide saturable absorber.)

the unstable pulses with the energy of a few nanojoules initiated the laser-driven self-exfoliation of the bulk GO film, which produced a visible plasma plume. This observation is considered to be related to the nanojoule pulse laser drilling by forming a short plasma plume [33,34] and further plasma characterization is being pursued by the authors. Once the GO multi-layer film was formed by the laser-driven self-exfoliation, we did not observe any subsequent laser drilling processes and we immediately obtained a very stable *Q* switching. Figure 2(c) shows an SEM image of the multi-layer GO film after the laser-driven self-exfoliation. The blown-up SEM image clearly shows a unique concentric layered structure, which confirmed that the GO bulk film was exfoliated selectively over the fiber core by the laser pulses. The inset also shows that the core has a significantly thinner film than the cladding so that the light guided by the core was clearly visible using an optical microscope. See the inset of Fig. 2(c). We further pursued Raman spectroscopy for the self-exfoliated GO film on the fiber core and the results are shown in Fig. 2(d). Here we used the 514 nm line of an Ar^+ ion laser as the Raman pump. The Raman spectrum showed the characteristic peaks of GO film in the D and G bands near 1350 cm^{-1} and 1590 cm^{-1}, respectively. The intensity ratio of the two bands (I_D/I_G) was ~1.1, similar to prior GO Raman reports [35,36]. Consistent with prior reports [35,37], the bands near 2700 cm^{-1} and 2950 cm^{-1} were observed which correspond to 2D and D + G, respectively. The GO Raman spectrum indicates that no thermal damage is observed in the electric arc process. In previous Raman spectroscopic studies on GO multi-layer films, however, a systematic correlation between the spectral structure and the number of GO layers has not been provided to the best knowledge of the authors. Therefore, we could not estimate the number of GO layers based on the Raman spectra. However, the thickness of the laser exfoliated multi-layer GO film on the fiber core was estimated to be ~40 nm by measuring the Fabry–Perot transmission as discussed in Section 3.C.

B. Linear and Nonlinear Transmission Measurement

We first measured the linear transmission of GO bulk film deposited on a silica substrate as a reference using the same GO aqueous solution as in fiber samples. The film was deposited by the drop-casting method [38] and its linear transmission was measured in the UV–near-IR region using a spectrophotometer (Agilent Cary 5000). The transmission spectrum is shown in Fig. 3(a), which is consistent with prior reports [16,39,40]. We further investigated the nonlinear transmission of the GO multi-layer film on the fiber facet formed by the laser-driven self-exfoliation using an experimental setup shown in Fig. 3(b). The probe femtosecond laser had the center wavelength at $\lambda = 1550$ nm, the pulse repetition rate of 80 MHz, and the pulse duration of 80 fs. A variable optical attenuator adjusted the optical power of the probe laser. Figure 3(c) shows the normalized transmission through the all-fiber GO-SA versus the input laser peak intensity.

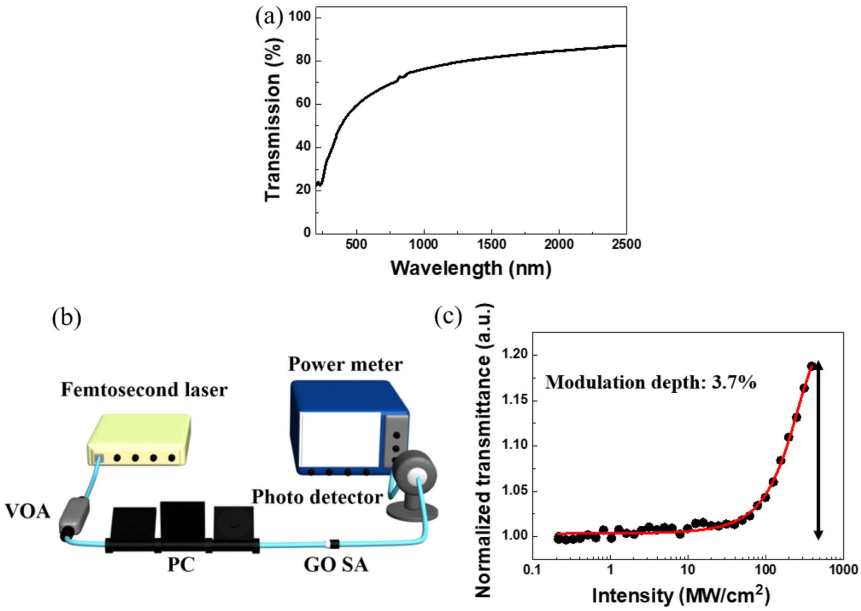

Fig. 3. (a) Linear transmission spectrum of GO bulk film on a silica substrate. (b) The measurement setup for the nonlinear transmission of the GO-SA formed by the laser-driven self-exfoliation process. (c) Nonlinear transmission of the GO-SA as a function of the input laser intensity. (GO-SA, graphene oxide saturable absorber; VOA, variable optical attenuator; PC, polarization controller.)

Within the available power of the probe laser, we did not observe the saturation of the transmission, yet we were able to fit the SA transmission equation [41]:

$$T = 1 - \frac{\alpha_0}{a + \frac{I}{I_{sat}}} - \alpha_{ns}, \quad (1)$$

where α_{ns} is the saturable loss, α_0 is the modulation depth, I is the incident light intensity, and I_{sat} is the saturation intensity. The modulation depth was estimated to be ~3.7%, which is comparable to prior reports for a few-layer GO film [14].

We further investigated the insertion loss (IL) of the multi-layer GO-SA keeping the distance from the other bare SMF at ~8 μm. The IL of the multi-layer GO-SA was measured to be ~0.6 dB in the L-band and its polarization-dependent loss (PDL) was ~0.3 dB. Note that the IL of multi-layer GO-SA was significantly lower than that of GO bulk film on the fiber facet formed by the electric arc, ~1.2 dB. This low IL of our GO-SA allowed an efficient Q switching in the L-band where the optical gain is inherently lower than that of the C-band [42]. The PDL of the GO bulk film device was ~0.4 dB, which was also slightly higher than that of multi-layer GO-SA.

C. All-Fiber Ring Laser Cavity and Its *Q* Switching Using a Multi-Layer GO-SA

The prepared multi-layer GO-SA was inserted in a ring laser cavity as schematically shown in Fig. 4. In the experiments, the total cavity length was ~5 m and the total net cavity dispersion was adjusted to be −0.07 ps^2. The gain medium was a commercial EDF Er80-8/125 from Liekki and its length was 1.5 m to shift the gain toward the L-band. We initially optimized the EDF length and the pump power in the ring cavity to obtain CW lasing at the center wavelength of $\lambda = 1604$ nm in the L-band without using the GO-SA. This cavity condition suppressed the optical gain in the C-band.

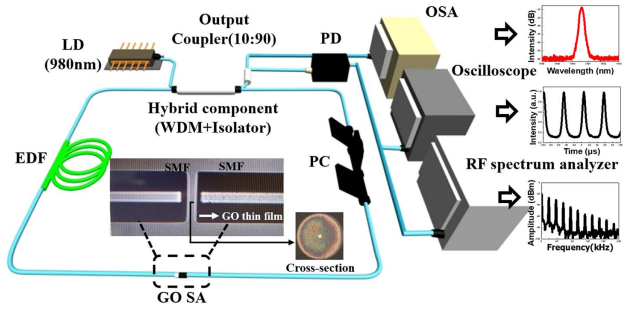

Fig. 4. Schematic diagram of Q switching experimental setup using the all-fiber GO-SA. The output of the laser was monitored in the wavelength spectral domain, RF domain, and time domain. (GO-SA, graphene oxide multi-layer film saturable absorber; LD, laser diode; EDF, erbium-doped fiber; PD, photodetector; PC, polarization controller; hybrid component, an integrated wavelength-division multiplexer and isolator; OSA, optical spectrum analyzer.)

When our GO-SA was inserted in the laser cavity it further increased the optical loss, which shifted the optical gain toward a shorter wavelength within the L-band. The Fabry–Perot nature of our GO-SA acted as a bandpass filter around $\lambda = 1600.5$ nm. By combining the optical gain, its shift by GO-SA loss, and the Fabry–Perot nature of the GO-SA, we were able to achieve Q switching in the L-band. The EDF was pumped using a 980 nm LD through a hybrid component composed of an isolator and a 980/1550 nm WDM. A polarization controller was used to adjust the round-trip polarization state in the fiber ring cavity. An output coupler with a power ratio of 10:90 was used where the 10% port served as the laser output port. An optical spectrum analyzer (Agilent 86140B), a radio-frequency (RF) spectrum analyzer (Keysight N9320B),

and a digital oscilloscope (Tektronix TDS744A) were used to characterize the laser output data in the spectral domain, the frequency domain, and the time domain, respectively.

3. EXPERIMENTAL RESULTS

A. Graphene Oxide Bulk Film Device in a Ring Laser Cavity

We started the laser experiment using a fiber device with the GO bulk film deposited by the electric arc (the middle figure of Fig. 1 inset). As we slowly increased the pump power toward ~149 mW, we could observe a sporadic mixture of the unstable Q switching and CW lasing. The lasing characteristics were measured by using an optical spectrum analyzer, an RF spectrum analyzer, and an oscilloscope, and the results are summarized in Fig. 5. As shown in Fig. 5(a), the optical spectra fluctuated randomly between the CW lasing and the unstable pulsing where the spectra were found to be broadened. The RF spectra were even more fluctuating, as shown in Fig. 5(b). In the case of CW lasing, there were no detectable peaks, while in the unstable Q-switched lasing we could observe peaks at the harmonics of 15–17 kHz with the signal-to-noise ratio (SNR) less than 20.5 dB.

The oscilloscope trace of one of the unstable pulse trains was recorded in the oscilloscope, as shown in Fig. 5(b) inset. The pulse width varied sporadically from a few microseconds to a few tens of microseconds along with fluctuating peak intensities. The pulses also showed a significant pedestal that decayed in time. We estimated the average energy of the unstable pulses to be in the range of nanojoule.

B. Graphene Oxide Multi-Layer Film Saturable Absorber in a Ring Laser Cavity

When we further increased the pump laser to over 149 mW, the energy and the peak power of the unstable pulse grew sufficiently to generate a plasma plume with a visible spark on the GO bulk film. It has been well understood that the plasma plume generated by a nanosecond laser serves as a direct sign of laser ablation in material processing [43,44]. In our laser-driven self-exfoliation process, the unstable nanojoule laser pulses within the EDFL cavity were interacting with GO bulk film and ablated it to result in a significantly thinner GO multi-layer film on the fiber core; see Fig. 2(c).

Immediately after the laser-driven self-exfoliation, the multi-layer GO-SA produced very stable and robust Q-switched pulse trains in a wide range of pump laser power, and the results are summarized in Figs. 6(a)–6(c) for the pump power of 194 mW. The optical spectrum is shown in Fig. 6(a) with the peak wavelength at $\lambda = 1600.5$ nm, which is the longest wavelength in Q-switched EDFL as summarized in Tables 1 and 2. It is also noted that the peak wavelength of the laser slightly decreased as the stable Q switching reached, as shown in the inset of Fig. 6(a). The RF spectrum in Fig. 6(b) showed a clear peak at $f = 17.8$ kHz with an SNR of 42.4 dB, which indicated the high stability of laser pulses. Symmetric pulses with a duration of 7.8 μs without prominent pedestals were observed in the oscilloscope as in Fig. 6(c). The peak-to-peak pulse period of 55.5 μs was consistent with the measured pulse repetition rate of 17.8 kHz.

Using the multi-layer GO-SA we measured the laser characteristics for various pump powers, and the results are summarized in Figs. 6(d)–6(f). It is noted that the repetition rate increased from 6.3 to 17.8 kHz, while the pulse width decreased from 24.0 to 7.8 μs in the pump power range. The output power linearly increased from 0.3 to 2.3 mW, while the pulse energy increased from 47.6 nJ and then saturated to 128.1 nJ. The pulse duty cycle decreased from 158.0 μs to 55.5 μs, and the corresponding peak power increased from 1.8 mW to 15.4 mW. These pump-power-dependent properties were consistent with those of prior Q-switched EDFLs [22–25]. However, we did not observe any significant change in the lasing wavelength within the pump power range. This is attributed to the Fabry–Perot nature of our multi-layer GO-SA working as a spectral filter, which is explained in the next section.

C. Fabry–Perot Spectral Selectivity of the Fabricated Multi-Layer GO-SA

The multi-layer GO-SA shown in Fig. 7(a) was found to simultaneously function as a Fabry–Perot filter, which locked the lasing wavelength. We measured transmission and reflection of the fabricated multi-layer GO-SA using the experimental setup in Fig. 7(a), where we used a supercontinuum light source (NKT Photonics, EXR-15), a fiber-optic circulator (Thorlabs, 1525–1610 nm, SMF, FC/APC), an optical spectrum analyzer (Agilent, 86140B), and an optical power meter. Here the multi-layer GO deposited fiber facet and a bare SMF facet were aligned axially with a gap $d = 8$ μm. We observed typical Fabry–Perot interference patterns in both the transmission and reflection spectra which were attributed to the optical path difference caused by the reflection at the multi-layer GO

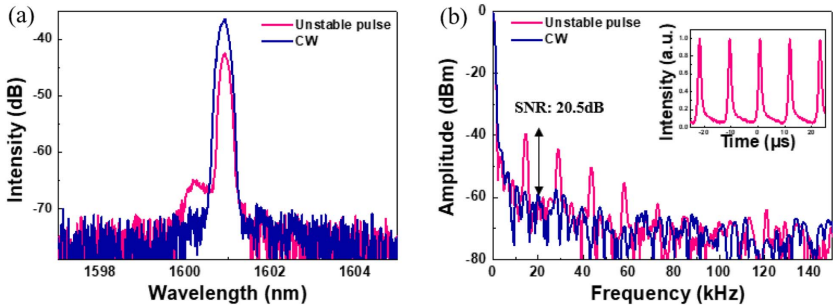

Fig. 5. Lasing characteristics for the bulk GO film device in the ring laser cavity: (a) optical spectra, (b) RF spectra and the oscilloscope trace in the inset. Here the pump laser power was ~149 mW.

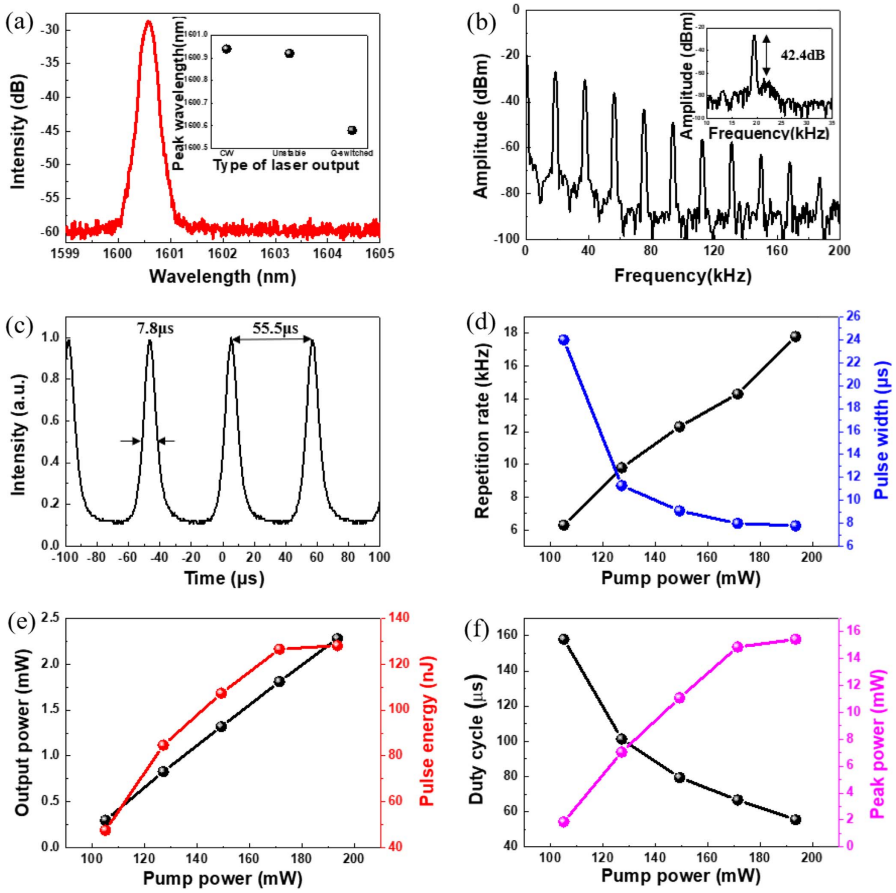

Fig. 6. Lasing characteristics of the *Q*-switched EDFL using the multi-layer GO-SA. (a) Optical spectrum (the inset shows the peak wavelength of the output laser for CW, unstable pulsing, and stable *Q*-switched pulsing); (b) RF spectrum; (c) oscilloscope trace of the pulse train. (d) Pulse repetition rate and pulse width as functions of the pump power; (e) output power and pulse energy as functions of the pump power. (f) Duty cycle and peak power as functions of the pump power.

film deposited on the fiber core. See the arrows in the inset of Fig. 7(a). We simulated the Fabry–Perot filter structure using COMSOL Multiphysics assuming the refractive index of ∼2 [45] and thickness of ∼40 nm for the multi-layer GO film. The simulation results and experimental measurements showed a good agreement as in Fig. 7(b). Transmission spectra had a free spectral range of ∼145 nm and a transmission peak at $\lambda\sim$ 1600 nm, which coincide with the laser output position in our experiments. We confirmed that the fixed lasing wavelength of the *Q*-switched laser against pump power variations was attributed to the Fabry–Perot filter nature of our multi-layer GO-SA.

In Table 1, we compared the performance of previous *Q*-switched EDFLs employing GO-SA with our results. In terms of the lasing wavelength, all of the previous results have been confined to the C-band. This spectral limit has been attributed to the significantly higher insertion loss of prior GO-SAs, which can be compensated only by the inherently higher gain in the C-band. Our GO-SA showed a very low insertion loss of 0.6 dB to enable utilization of the lower gain in the L-band. In terms of the pulse width, our laser provided a wide range from 7.8 to 24.0 μs. The maximum peak power of the *Q*-switched pulse in our work showed the largest

Table 1. *Q*-Switched EDFLs Based on Graphene Oxide Saturable Absorbers

Material	Types of SA	Deposition Method	Wavelength (nm)	Pulse Width (μs)	Max. Peak Power (mW)	Pulse Energy (nJ)	Repetition Rate (kHz)	Ref.
GO	SPF[a]	Spray method	1558	2.12	–	–	8.96	[22]
GO	PCF[b]	Solution filled inside the PCF	1553.42–1561.67	–	0.167	8.98	16	[23]
GO	End face	Polymer-based thin film	1558–1570	6.6–13.7	–	19.2–61.3	22–61	[24]
GO	End face	Optical deposition	1531.6	20.44–61.2	9.3	46.6–145.0	21.5–68.7	[25]
GO	End face	Laser induced self-exfoliation	1600.5	7.8–24.0	15.4	47.6–128.1	6.3–17.8	This work

[a]SPF: side polished fiber.
[b]PCF: photonic crystal fiber.

Table 2. Performance Comparison of the Present Result to Recent *Q*-Switched EDFLs Incorporating Other Materials in the L-Band

Material	Types of SA	Method	Wavelength (nm)	Min. Pulse Width (μs)	Max. Pulse Energy (nJ)	Max. Repetition Rate (kHz)	Max. Output Power (mW)	Ref.
ZnO	End face	Polymer-based thin film	1536–1586	4.5	39.9	28.9	1.2	[46]
In_2Se_3	End face	Mechanical exfoliation	1533–1573	2.2	13.5	52	0.7	[47]
TiO_2	End face	Polymer-based thin film	1534–1570	2.7	–	22.2	0.087	[48]
Ag	End face	Polymer-based thin film	1552.9–1580.2	11.9	–	10.5	0.044	[49]
GO	End face	Laser induced self-exfoliation	1600.5	7.8	128.1	17.8	2.3	This work

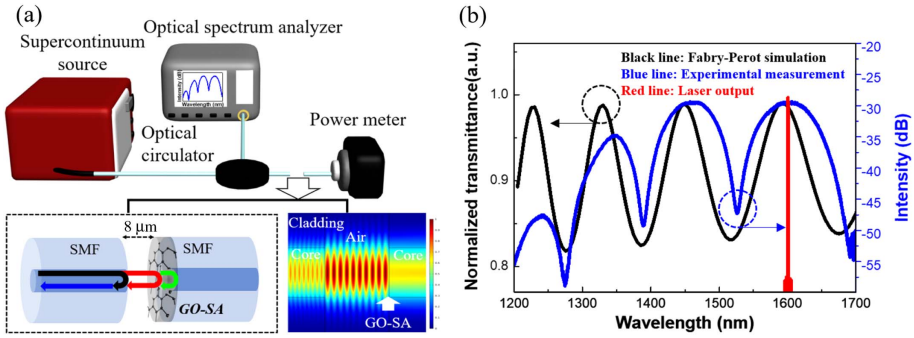

Fig. 7. (a) Schematic diagram of transmission measurements for the fabricated multi-layer GO-SA with the gap of ~8 μm. (b) Fabry–Perot filter simulation (black line), experimental measurements (blue line), and the laser output (red line).

value of 15.4 mW, which is a more than 50% increase in comparison to prior reports [25].

We further compared the performances of L-band *Q* switching using other nonlinear optical materials with our study in Table 2. These films have been deposited on the fiber end face similar to our study, which allowed a fair comparison with our laser. It is noted that all the prior reports [46–49] have experimentally demonstrated *Q* switching only in the shorter wavelength region of the L-band and we obtained the longest wavelength $\lambda > 1600$ nm by using our GO-SA. In terms of the maximum pulse energy, our study showed more than threefold (300%) increase in comparison to prior reports. The average output power of our laser showed a nearly twofold increase. These outperforming laser characteristics were attributed to our unique multi-layer GO-SA fabricated by the laser-driven self-exfoliation method. Promising nonlinear optic materials have been recently reported [50–54], which enabled efficient laser pulse generation in various optical cavities. In comparison to those new materials with an inherently high optical nonlinearity, GO has a moderate nonlinearity but provides a good dispersion capability in a colloidal suspension and the hydrophilic nature compatible with the silica surface of the optical fiber, which served as a good starting material to explore our new deposition process—the proposed laser-driven self-exfoliation method. In recent years, applications of microsecond pulsed laser have been rapidly widened in the military, medical, and industrial fields [55–57], and our study could further increase the application in the L-band spectral range that has not been reached by prior lasers.

In the pursuit of an optimal saturable absorber to generate short light pulses, various types of materials are being explored including 2D materials such as graphene, TMDs, tellurene, black phosphorus, and boron nitride [9–11,2–5,53,54,58], to name a few. However, systematic comparisons of these materials, especially when embedded in fiber-optic devices, have been hindered due to lack of a proper platform that can provide precise deposition of thin films over the fiber surface in a very reliable and repeatable manner, while maintaining the genuine optical nonlinearity of the materials. In recent years, homogeneous colloidal suspensions of nanoflakes made of these materials have been commercially available and our method consuming only a drop of the colloidal precursor on a fiber facet can further expand its usages over those new materials. We successfully deposited one of the TMDs on the fiber facet utilizing our method, which will be reported in a separate paper, and we confirmed its high potential as a fiber-optic device platform technology for novel nonlinear optical materials.

4. CONCLUSION

We successfully developed a new all-fiber saturable absorber by depositing the multi-layer GO film selectively on the core of an optical fiber facet by applying an electrical arc and subsequently the laser-driven self-exfoliation. We experimentally measured the nonlinear transmission of the all-fiber GO-SA to obtain the optical modulation depth of 3.7%. The IL was as low as ~0.6 dB and its polarization-dependent loss was ~0.3 dB. Using this all-fiber multi-layer GO-SA in an Er-doped fiber ring laser cavity, we generated stable pulse trains at $\lambda = 1600.5$ nm, the longest *Q*-switched laser wavelength in the L-band regimes by optimizing optical gain, cavity loss, and Fabry–Perot filter. When the pump power increased from

105.2 to 193.6 mW, the repetition rate increased from 6.3 to 17.8 kHz, the pulse width decreased from 24.0 to 7.8 μs, and the average output power increased from 0.3 to 2.3 mW. The proposed laser-driven self-exfoliation method consumed only a few nanoliters of the precursor solution and the deposition was obtained within a few milliseconds in the electric arc followed by the *Q*-switched laser pulse ablation, which provided the shortest processing time. The proposed method could be further applied to various novel two-dimensional materials to provide a new avenue of nonlinear optics to generate various pulsed lasers.

Funding. National Research Foundation of Korea (NRF-2019R1A2C2011293).

Disclosures. The authors declare no conflicts of interest.

REFERENCES

1. S. Hong, F. Lédée, J. Park, S. Song, H. Lee, Y. S. Lee, B. Kim, D. I. Yeom, E. Deleporte, and K. Oh, "Mode-locking of all-fiber lasers operating at both anomalous and normal dispersion regimes in the C- and L-bands using thin film of 2D perovskite crystallites," Laser Photonics Rev. **12**, 1800118 (2018).
2. R. Khazaeizhad, S. H. Kassani, H. Jeong, D.-I. Yeom, and K. Oh, "Mode-locking of Er-doped fiber laser using a multilayer MoS_2 thin film as a saturable absorber in both anomalous and normal dispersion regimes," Opt. Express **22**, 23732–23742 (2014).
3. R. Khazaeinezhad, T. Nazari, H. Jeong, K. J. Park, B. Y. Kim, D.-I. Yeom, and K. Oh, "Passive *Q*-switching of an all-fiber laser using WS_2-deposited optical fiber taper," IEEE Photonics J. **7**, 1503507 (2015).
4. R. Khazaeinezhad, S. H. Kassani, H. Jeong, K. J. Park, B. Y. Kim, D.-I. Yeom, and K. Oh, "Ultrafast pulsed all-fiber laser based on tapered fiber enclosed by few-layer WS_2 nanosheets," IEEE Photonics Technol. Lett. **27**, 1581–1584 (2015).
5. R. Khazaeinezhad, S. H. Kassani, H. Jeong, T. Nazari, D.-I. Yeom, and K. Oh, "Mode-locked all-fiber lasers at both anomalous and normal dispersion regimes based on spin-coated MoS_2 nano-sheets on a side-polished fiber," IEEE Photonics J. **7**, 1500109 (2015).
6. Y. Meng, G. Semaan, M. Salhi, A. Niang, K. Guesmi, Z.-C. Luo, and F. Sanchez, "High power L-band mode-locked fiber laser based on topological insulator saturable absorber," Opt. Express **23**, 23053–23058 (2015).
7. J. Nicholson, R. Windeler, and D. DiGiovanni, "Optically driven deposition of single-walled carbon-nanotube saturable absorbers on optical fiber end-faces," Opt. Express **15**, 9176–9183 (2007).
8. M. Chernysheva, C. Mou, R. Arif, M. AlAraimi, M. Rümmeli, S. Turitsyn, and A. Rozhin, "High power *Q*-switched thulium doped fibre laser using carbon nanotube polymer composite saturable absorber," Sci. Rep. **6**, 24220 (2016).
9. Q. Bao, H. Zhang, Y. Wang, Z. Ni, Y. Yan, Z. X. Shen, K. P. Loh, and D. Y. Tang, "Atomic-layer graphene as a saturable absorber for ultrafast pulsed lasers," Adv. Funct. Mater. **19**, 3077–3083 (2009).
10. G. Xie, J. Ma, P. Lv, W. Gao, P. Yuan, L. Qian, H. Yu, H. Zhang, J. Wang, and D. Tang, "Graphene saturable absorber for *Q*-switching and mode locking at 2 μm wavelength," Opt. Mater. Express **2**, 878–883 (2012).
11. A. Martinez and Z. Sun, "Nanotube and graphene saturable absorbers for fibre lasers," Nat. Photonics **7**, 842–845 (2013).
12. Z. Liu, Y. Wang, X. Zhang, Y. Xu, Y. Chen, and J. Tian, "Nonlinear optical properties of graphene oxide in nanosecond and picosecond regimes," Appl. Phys. Lett. **94**, 021902 (2009).
13. Y. Zhu, S. Murali, W. Cai, X. Li, J. W. Suk, J. R. Potts, and R. S. Ruoff, "Graphene and graphene oxide: synthesis, properties, and applications," Adv. Mater. **22**, 3906–3924 (2010).
14. H.-R. Chen, C.-Y. Tsai, H.-M. Cheng, K.-H. Lin, and W.-F. Hsieh, "Passive mode locking of ytterbium-and erbium-doped all-fiber lasers using graphene oxide saturable absorbers," Opt. Express **22**, 12880–12889 (2014).
15. X. Li, K. Wu, Z. Sun, B. Meng, Y. Wang, Y. Wang, X. Yu, X. Yu, Y. Zhang, and P. P. Shum, "Single-wall carbon nanotubes and graphene oxide-based saturable absorbers for low phase noise mode-locked fiber lasers," Sci. Rep. **6**, 25266 (2016).
16. X. Li, Y. Tang, Z. Yan, Y. Wang, B. Meng, G. Liang, H. Sun, X. Yu, Y. Zhang, and X. Cheng, "Broadband saturable absorption of graphene oxide thin film and its application in pulsed fiber lasers," IEEE J. Sel. Top. Quantum Electron. **20**, 441–447 (2014).
17. Z.-B. Liu, X. He, and D. Wang, "Passively mode-locked fiber laser based on a hollow-core photonic crystal fiber filled with few-layered graphene oxide solution," Opt. Lett. **36**, 3024–3026 (2011).
18. G. Sobon, J. Sotor, J. Jagiello, R. Kozinski, M. Zdrojek, M. Holdynski, P. Paletko, J. Boguslawski, L. Lipinska, and K. M. Abramski, "Graphene oxide vs. reduced graphene oxide as saturable absorbers for Er-doped passively mode-locked fiber laser," Opt. Express **20**, 19463–19473 (2012).
19. D. Steinberg, R. M. Gerosa, F. N. Pellicer, J. D. Zapata, S. H. Domingues, E. A. T. de Souza, and L. A. Saito, "Graphene oxide and reduced graphene oxide as saturable absorbers onto D-shaped fibers for sub 200-fs EDFL mode-locking," Opt. Mater. Express **8**, 144–156 (2018).
20. J. Xu, J. Liu, S. Wu, Q.-H. Yang, and P. Wang, "Graphene oxide mode-locked femtosecond erbium-doped fiber lasers," Opt. Express **20**, 15474–15480 (2012).
21. J. Boguslawski, J. Sotor, G. Sobon, R. Kozinski, K. Librant, M. Aksienionek, L. Lipinska, and K. M. Abramski, "Graphene oxide paper as a saturable absorber for Er-and Tm-doped fiber lasers," Photon. Res. **3**, 119–124 (2015).
22. J. Lee, J. Koo, P. Debnath, Y. Song, and J. Lee, "A *Q*-switched, mode-locked fiber laser using a graphene oxide-based polarization sensitive saturable absorber," Laser Phys. Lett. **10**, 035103 (2013).
23. H. Ahmad, M. Soltanian, M. Alimadad, and S. Harun, "Stable narrow spacing dual-wavelength *Q*-switched graphene oxide embedded in a photonic crystal fiber," Laser Phys. **24**, 105101 (2014).
24. N. Aziz, Z. Jusoh, M. Lokman, M. Yasin, E. Hanafi, and S. Harun, "*Q*-switched erbium-doped fiber laser with graphene oxide embedded in PMMA film," Digest J. Nanomater. Biostruct. **12**, 325–330 (2017).
25. H. Ahmad, F. Muhammad, M. Zulkifli, and S. Harun, "Graphene-oxide-based saturable absorber for all-fiber *Q*-switching with a simple optical deposition technique," IEEE Photonics J. **4**, 2205–2213 (2012).
26. R. Khazaeinezhad, S. H. Kassani, T. Nazari, H. Jeong, J. Kim, K. Choi, J.-U. Lee, J. H. Kim, H. Cheong, and D.-I. Yeom, "Saturable optical absorption in MoS_2 nano-sheet optically deposited on the optical fiber facet," Opt. Commun. **335**, 224–230 (2015).
27. H. Ahmad, N. Ruslan, M. Ismail, S. Reduan, C. Lee, S. Sathiyan, S. Sivabalan, and S. W. Harun, "Passively *Q*-switched erbium-doped fiber laser at C-band region based on WS_2 saturable absorber," Appl. Opt. **55**, 1001–1005 (2016).
28. Y. Chen, G. Jiang, S. Chen, Z. Guo, X. Yu, C. Zhao, H. Zhang, Q. Bao, S. Wen, and D. Tang, "Mechanically exfoliated black phosphorus as a new saturable absorber for both *Q*-switching and mode-locking laser operation," Opt. Express **23**, 12823–12833 (2015).
29. H. Mu, S. Lin, Z. Wang, S. Xiao, P. Li, Y. Chen, H. Zhang, H. Bao, S. P. Lau, and C. Pan, "Black phosphorus-polymer composites for pulsed lasers," Adv. Opt. Mater. **3**, 1447–1453 (2015).
30. M. A. Ismail, S. W. Harun, H. Ahmad, and M. C. Paul, *Passive Q-switched and Mode-locked Fiber Lasers Using Carbon-based Saturable Absorbers* (IntechOpen, 2016).
31. B. Janczuk and A. Zdziennicka, "A study on the components of surface free energy of quartz from contact angle measurements," J. Mater. Sci. **29**, 3559–3564 (1994).
32. W. Lim, Y. Yap, W. Chong, C. Pua, N. Huang, R. De La Rue, and H. Ahmad, "Graphene oxide-based waveguide polariser: from thin film to quasi-bulk," Opt. Express **22**, 11090–11098 (2014).
33. K.-H. Leitz, B. Redlingshöfer, Y. Reg, A. Otto, and M. Schmidt, "Metal ablation with short and ultrashort laser pulses," Phys. Proc. **12**, 230–238 (2011).

34. G. G. Gladush and I. Smurov, *Physics of Laser Materials Processing: Theory and Experiment* (Springer, 2011).
35. H. N. Tien, J. S. Chung, and S. H. Hur, "Fabrication of a novel 2D-graphene/2D-NiO nanosheet-based hybrid nanostructure and its use in highly sensitive NO2 sensors," Sens. Actuators B **185**, 701–705 (2013).
36. S. Jaworski, M. Wierzbicki, E. Sawosz, A. Jung, G. Gielerak, J. Biernat, H. Jaremek, W. Łojkowski, B. Woźniak, and J. Wojnarowicz, "Graphene oxide-based nanocomposites decorated with silver nanoparticles as an antibacterial agent," Nanosc. Res. Lett. **13**, 116 (2018).
37. S. K. Tiwari, G. Hatui, R. Oraon, A. De Adhikari, and G. C. Nayak, "Mixing sequence driven controlled dispersion of graphene oxide in PC/PMMA blend nanocomposite and its effect on thermo-mechanical properties," Curr. Appl. Phys. **17**, 1158–1168 (2017).
38. S. R. Dugasani, B. Paulson, T. Ha, T. S. Jung, B. Gnapareddy, J. A. Kim, T. Kim, H. J. Kim, J. H. Kim, and K. Oh, "Fabrication and opto-electronic characterisation of lanthanide-and metal-ion-doped DNA thin films," J. Phys. D **51**, 285301 (2018).
39. P. Raturi and J. Singh, "Sunlight-driven eco-friendly smart curtain based on infrared responsive graphene oxide-polymer photoactuators," Sci. Rep. **8**, 3687 (2018).
40. M. Mazurkiewicz-Pawlicka, M. Nowak, A. Malolepszy, A. Witowski, D. Wasik, Y. Hu, and L. Stobinski, "Graphene oxide with controlled content of oxygen groups as a filler for polymer composites used for infrared radiation shielding," Nanomaterials **10**, 32 (2020).
41. A. Martinez and S. Yamashita, "Carbon nanotube-based photonic devices: applications in nonlinear optics," in *Carbon Nanotubes Applications on Electron Devices* (InTech, 2011), pp. 367–386.
42. X. Zhao, Z. Zheng, L. Liu, Y. Liu, Y. Jiang, X. Yang, and J. Zhu, "Switchable, dual-wavelength passively mode-locked ultrafast fiber laser based on a single-wall carbon nanotube modelocker and intracavity loss tuning," Opt. Express **19**, 1168–1173 (2011).
43. A. H. Hamad, "Effects of different laser pulse regimes (nanosecond, picosecond and femtosecond) on the ablation of materials for production of nanoparticles in liquid solution," in *High Energy and Short Pulse Lasers* (InTech, 2016), pp. 305–325.
44. A. Matsumoto, H. Ohba, M. Toshimitsu, K. Akaoka, A. Ruas, I. Wakaida, T. Sakka, and S. Yae, "Enhancement of molecular formation in fiber-optic laser ablation with a long nanosecond pulsed laser," Spectrochim. Acta B **155**, 56–60 (2019).
45. V. Kravets, O. Marshall, R. Nair, B. Thackray, A. Zhukov, J. Leng, and A. Grigorenko, "Engineering optical properties of a graphene oxide metamaterial assembled in microfluidic channels," Opt. Express **23**, 1265–1275 (2015).
46. H. Ahmad, C. Lee, M. A. Ismail, Z. Ali, S. Reduan, N. Ruslan, and S. W. Harun, "Tunable *Q*-switched fiber laser using zinc oxide nanoparticles as a saturable absorber," Appl. Opt. **55**, 4277–4281 (2016).
47. H. Ahmad, A. Z. Zulkifli, M. Yasin, M. F. Ismail, and K. Thambiratnam, "In_2Se_3 saturable absorber for generating tunable *Q*-switched outputs from a bismuth-erbium doped fiber laser," Laser Phys. Lett. **15**, 115105 (2018).
48. H. Ahmad, S. A. Reduan, N. Ruslan, C. S. J. Lee, M. Z. Zulkifli, and K. Thambiratnam, "Tunable *Q*-switched erbium-doped fiber laser in the C-band region using nanoparticles (TiO_2)," Opt. Commun. **435**, 283–288 (2019).
49. H. Ahmad, N. Ruslan, Z. Ali, S. Reduan, C. Lee, R. Shaharuddin, N. Nayan, and M. A. Ismail, "Ag-nanoparticle as a *Q* switched device for tunable C-band fiber laser," Opt. Commun. **381**, 85–90 (2016).
50. Z. Xie, F. Zhang, Z. Liang, T. Fan, Z. Li, X. Jiang, H. Chen, J. Li, and H. Zhang, "Revealing of the ultrafast third-order nonlinear optical response and enabled photonic application in two-dimensional tin sulfide," Photon. Res. **7**, 494–502 (2019).
51. L. Wu, Z. Xie, L. Lu, J. Zhao, Y. Wang, X. Jiang, Y. Ge, F. Zhang, S. Lu, and Z. Guo, "Few-layer tin sulfide: a promising black-phosphorus-analogue 2D material with exceptionally large nonlinear optical response, high stability, and applications in all-optical switching and wavelength conversion," Adv. Opt. Mater. **6**, 1700985 (2018).
52. C. Xing, Z. Xie, Z. Liang, W. Liang, T. Fan, J. S. Ponraj, S. C. Dhanabalan, D. Fan, and H. Zhang, "2D nonlayered selenium nanosheets: facile synthesis, photoluminescence, and ultrafast photonics," Adv. Opt. Mater. **5**, 1700884 (2017).
53. Y. Wang, W. Huang, C. Wang, J. Guo, F. Zhang, Y. Song, Y. Ge, L. Wu, J. Liu, and J. Li, "An all-optical, actively *Q*-switched fiber laser by an antimonene-based optical modulator," Laser Photonics Rev. **13**, 1800313 (2019).
54. J. Zheng, X. Tang, Z. Yang, Z. Liang, Y. Chen, K. Wang, Y. Song, Y. Zhang, J. Ji, and Y. Liu, "Few-layer phosphorene-decorated microfiber for all-optical thresholding and optical modulation," Adv. Opt. Mater. **5**, 1700026 (2017).
55. D. H. Titterton, *Military Laser Technology and Systems* (Artech House, 2015).
56. A. Badawi, M. A. Tome, A. Atteya, N. Sami, and I. A. Morsy, "Retrospective analysis of non-ablative scar treatment in dark skin types using the sub-millisecond Nd:YAG 1,064 nm laser," Lasers Surg. Med. **43**, 130–136 (2011).
57. N. B. Dahotre and S. Harimkar, *Laser Fabrication and Machining of Materials* (Springer, 2008).
58. L. Li, X. Yang, L. Zhou, W. Xie, Y. Bai, G. Ye, Y. Shen, Z. Lv, H. Zhang, and M. Chen, "BN as a saturable absorber for a passively mode-locked 2 μm solid-state laser," Physica Status Solidi (RRL) **13**, 1800482 (2019).